Effect of Geometry on Thermoelastic Instability in Disk Brakes and Clutches

Yun-Bo Yi

Shuqin Du

J. R. Barber

Department of Mechanical Engineering
and Applied Mechanics,
University of Michigan,
Ann Arbor, MI 48109-2125

J. W. Fash

Ford Scientific Research Laboratories,
Dearborn, MI 48121-2053

The finite element method is used to reduce the problem of thermoelastic instability (TEI) for a brake disk to an eigenvalue problem for the critical speed. Conditioning of the eigenvalue problem is improved by performing a preliminary Fourier decomposition of the resulting matrices. Results are also obtained for two-dimensional layer and three-dimensional strip geometries, to explore the effects of increasing geometric complexity on the critical speeds and the associated mode shapes. The hot spots are generally focal in shape for the three-dimensional models, though modes with several reversals through the width start to become dominant at small axial wavenumbers n, including a "thermal banding" mode corresponding to n = 0. The dominant wavelength (hot spot spacing) and critical speed are not greatly affected by the three-dimensional effects, being well predicted by the two-dimensional analysis except for banding modes. Also, the most significant deviation from the two-dimensional analysis can be approximated as a monotonic interpolation between the two-dimensional critical speeds for plane stress and plane strain as the width of the sliding surface is increased. This suggests that adequate algorithms for design against TEI could be developed based on the simpler two-dimensional analysis.

1 Introduction

The frictional heat generated during sliding causes thermoelastic expansion that affects the distribution of contact pressure. The resulting thermomechanical feedback is unstable if the sliding speed is sufficiently high, leading to the development of non-uniform contact pressure and local high temperatures known as "hot spots." This non-uniformity also tends to cause a low frequency vibration known in the automotive disk brake community as "hot roughness" or "hot judder." This is a significant source of customer warranty claims and has resulted in an increased interest in the subject in recent years (Kreitlow et al., 1985; Inoue, 1986; Zagrodzki, 1990; Anderson and Knapp, 1990; Lee and Dinwiddie, 1998).

The mechanism of thermoelastic instability or "TEI" was first explained by Barber (1967, 1969), who also described experimental observations of the resulting hot spots in railway brakes. Dow and Burton (1972) used a perturbation method to analyse the process and demonstrated that there is a critical sliding speed above which the system becomes unstable. In a subsequent paper, Burton et al. (1973) developed expressions for the critical speed in the sliding of two thermoelastic half-planes.

These idealized treatments provide a useful indication of the nature of the phenomenon and the effect of material properties on the critical speed, but the predicted critical speeds are typically significantly higher than those observed experimentally. A significant step towards explaining this discrepancy was made by Lee and Barber (1993), who analysed the problem of a layer sliding between two half-planes. They found that the finite layer thickness had the effect of predisposing the system to an antisymmetric mode shape with hot spots alternating on the two sliding surfaces. The wavelength and hence the spacing of hot spots was linked to the thickness of the layer and the critical speed was considerably lower than that predicted by the half-plane model. All of these predictions show quite good agreement with experimental results, despite the considerable simplifications implicit in the layer model, and Lee's analysis is quite well suited to implementation in brake design procedures (Hartsock et al., 1997). However, it is desirable to have some way of assessing the influence of other features of the brake geometry—notably the finite radial width of the brake disk and the axisymmetric (rather than two-dimensional) geometry.

Du et al. (1997) recently developed a finite element implementation of Burton's perturbation method which permits such an investigation for the case where only one of the sliding materials is a thermal conductor. In this limiting case, the stability boundary corresponds to the condition in which a non-trivial perturbation of the thermal and mechanical fields is neutrally stable and hence satisfies the steady-state equations of thermoelasticity. The most general such perturbation has N degrees of freedom corresponding to the nodal forces at the N contact nodes and hence the stability problem reduces to an $N \times N$ eigenvalue problem for the critical sliding speed.

In the present paper, we modify Du's method by making use of Fourier decomposition to partition the matrix and hence reduce the size of the eigenvalue problem. We also make use of the commercial FEA code ABAQUS, in place of the custom-made code described by Du et al. (1997), since this facilitates pre- and post-processing. The principal objective of the paper is to assess the likely error involved in using Lee's two-dimensional analytical solution to predict the critical speed and mode shape for a brake disk. The investigation will confirm that Lee's analysis provides an excellent approximation to the more accurate results in most cases.

2 Model Description

Lee and Barber (1993) determined the critical speed for an infinite two-dimensional layer sliding between two elastic half-planes. The layer, shown schematically in Fig. 1(a), is taken to represent the disk in a disk brake, while the half-planes (not shown in the figure) represent the friction pads. By contrast, the disk shown in Fig. 1(c) has an axisymmetric geometry and a finite radial width $w = r_2 - r_1$, where r_1, r_2 are the inner and outer radii respectively. An intermediate case is the strip model of Fig. 1(b), which is straight, but which has finite width w.

Contributed by the Tribology Division for publication in the JOURNAL OF TRIBOLOGY. Manuscript received by the Tribology Division July 7, 1998. Associate Technical Editor: T. C. Ovaert.

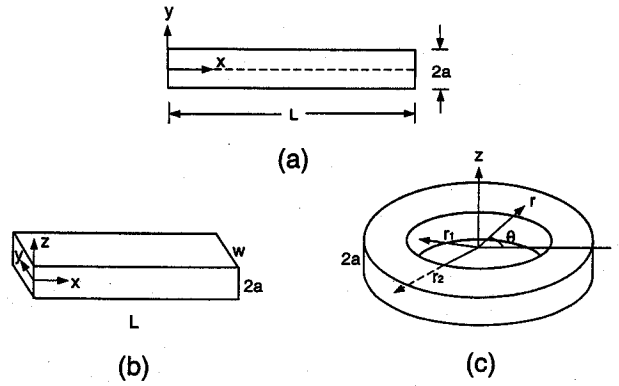

Fig. 1 Geometry of (*a*) the two-dimensional layer, (*b*) the three-dimensional strip, (c) the three-dimensional disk

The mathematical structure of the governing equations shows that all three geometries will support only Fourier modes—i.e. modes that vary with cos (mx) in Figs. 1(a, b) or with cos $(n\theta)$ in Fig. 1(c). Continuity considerations demand that n be an integer for the disk and a similar restriction can be imposed on the layer and strip models by choosing the wavelength $2\pi/m$ to be a submultiple of the mean disk circumference $\pi(r_1 + r_2)$. This also implies that we should impose symmetric boundary conditions on the ends $x = 0, L$ in Figs. 1(a, b).

There are several reasons why the stability behavior of the disk may differ from that of an equivalent layer

1. The disk is a three-dimensional structure and can support modes involving nonuniform pressure in the radial direction. By contrast, the layer model is two-dimensional and its use is equivalent to the assumption that pressure and temperature is independent of radius in Fig. 1(c). Experimental results show that hot spots are typically focal and hence show considerable radial variation.
2. The surfaces at $r = r_1, r_2$ are traction-free, whereas the layer model implies plane strain conditions on any such surfaces.
3. The disk supports circumferential or "hoop" stresses which have no counterpart in the layer geometry.
4. The sliding speed $V = \Omega r$, where Ω is the rotational speed, and hence it varies across the radial thickness. The best we can do with the layer model is to use the speed at the mean radius $r_m = (r_1 + r_2)/2$.

The first two of these features also occur in the strip model of Fig. 1(b).

In the interests of simplicity, and also to permit the use of the finite element method of Du et al. (1997), we assume that the friction pads are rigid nonconductors and that the shear tractions have no effect on the normal displacement at the contact surfaces. This latter assumption is exact when Poisson's ratio $\nu = 0.5$ and generally has a fairly small effect in frictional contact problems (Johnson, 1985).

3 Solution Method

The background to the method is fully described by Du et al. (1997) and will only be briefly outlined here. Since the pads are assumed to be nonconductors, the heat input q to the disk at the sliding surfaces is given by

$$q = fVp, \tag{1}$$

where p is the local contact pressure, f is the coefficient of friction, and V is the sliding speed. In the finite element implementation, p, q will be represented by a set of nodal heat fluxes q_i and forces p_i, $i = 1, N$ and Eq. (1) will be replaced by the vector equation

$$\mathbf{q} = fV\mathbf{p}. \tag{2}$$

The vectors $\mathbf{p}, \mathbf{q}$ are also related by the equations of steady-state linear thermoelasticity with appropriate thermal and mechanical boundary conditions on the remaining surfaces. We represent this linear relation in the generalized form

$$\mathbf{p} = \mathbf{A}\mathbf{q}. \tag{3}$$

We can then combine Eqs. (2), (3) to obtain

$$\mathbf{p} = fV\mathbf{A}\mathbf{p} \quad \text{or} \quad \mathbf{C}\mathbf{p} - fV\mathbf{p} = 0, \tag{4}$$

where $\mathbf{C} = \mathbf{A}^{-1}$. This constitutes a linear eigenvalue problem for the critical sliding speed V. Since the matrix $\mathbf{A}$ is of dimension $N \times N$, we anticipate N eigenvalues and a corresponding set of N eigenfunctions, which will describe the form of the temperature perturbation that occurs in the system. However, the stability of the system will be determined by the mode associated with the lowest eigenvalue.

3.1 Fourier Decomposition. The matrix $\mathbf{A}$ can be determined by solving a set of linear thermoelastic contact problems for any N linearly independent prescribed heat inputs $\mathbf{Q}^j$, $j = 1, N$. Thus, if the vector of nodal heat fluxes $\mathbf{q}^j$ produces nodal contact forces $\mathbf{p}^j$, it follows by linear superposition that $\mathbf{q} = \mathbf{Q}\mathbf{a}$ will produce $\mathbf{p} = \mathbf{P}\mathbf{a}$ where $\mathbf{Q}, \mathbf{P}$ are the matrices defined by

$$Q_{ij} = q_i^j; \quad P_{ij} = p_i^j \tag{5}$$

and $\mathbf{a}$ is any vector. We then have $\mathbf{a} = \mathbf{Q}^{-1}\mathbf{q}$, $\mathbf{p} = \mathbf{P}\mathbf{Q}^{-1}\mathbf{q}$ and hence

$$\mathbf{A} = \mathbf{P}\mathbf{Q}^{-1}. \tag{6}$$

However, the symmetries of the bodies illustrated in Fig. 1 ensure that the eigenfunctions of Eq. (4) will have Fourier form in the x- or θ-direction and it is therefore possible to partition the matrix $\mathbf{A}$ using Fourier decomposition, thus reducing the dimension of the resulting eigenvalue problem and aiding numerical efficiency and convergence.

3.1.1. The Two-Dimensional Problem. For the layer problem of Fig. 1(a), we first define the heat flux in the symmetric Fourier form

$$q(x) = \sum_{j=1}^{N} a_j \cos\left(\frac{\pi i x}{L}\right). \tag{7}$$

If the nodes are equally spaced on $0 < x < L$, so that $x_i = iL/N$, the nodal heat fluxes q_i are defined by

$$q_i = \int_0^L q(x)W_i(x)dx = B_{ij}\tilde{q}_j, \tag{8}$$

where $W_i(x)$ is the shape function,

$$B_{ij} = \cos\left(\frac{\pi j x_i}{L}\right) = \cos\left(\frac{\pi N x_j x_i}{L^2}\right) \tag{9}$$

and

$$\tilde{q}_j = \frac{L}{N}a_j. \tag{10}$$

A similar mode of representation is used for the contact pressure, such that the nodal contact force

$$p_i = \int_0^L p(x)W_i\,dx = B_{ij}\tilde{p}_j. \tag{11}$$

Substitution of these results into (3), yields

$$\mathbf{B}\tilde{\mathbf{p}} = \mathbf{AB}\tilde{\mathbf{q}} \tag{12}$$

and hence

$$\tilde{\mathbf{p}} = \mathbf{B}^{-1}\mathbf{AB}\tilde{\mathbf{q}} = \tilde{\mathbf{A}}\tilde{\mathbf{q}}, \tag{13}$$

where $\tilde{\mathbf{A}} = \mathbf{B}^{-1}\mathbf{AB}$.

We now use the finite element method to determine the contact pressure vector $\tilde{\mathbf{p}}$ due to the special heat flux vector $\tilde{q}_j = \delta_{jk}$, where δ_{jk} is the Kronecker delta. This is equivalent to a single term in Eq. (7) and hence, in view of the orthogonality property of the Fourier series, we anticipate that $\tilde{p}_j = c_k\delta_{jk}$, where c_k is a constant. In other words, the matrix $\tilde{\mathbf{A}}$ will be the diagonal matrix defined by

$$\tilde{A}_{jk} = c_k\delta_{jk} \tag{14}$$

and the c_k can be determined by making N such finite element runs with $j = 1, \ldots N$.

Applying $\mathbf{B}^{-1}$ to (4), we obtain

$$\tilde{\mathbf{p}} = fV\tilde{\mathbf{A}}\tilde{\mathbf{p}} \quad \text{or} \quad \tilde{p}_j = fVc_k\delta_{jk}\tilde{p}_k, \tag{15}$$

which has nontrivial solutions only for the critical sliding speeds

$$V = V_k = \frac{1}{fc_k}. \tag{16}$$

3.1.2 The Three-Dimensional Problem. For the three-dimensional problems of Figs. 1(*b*, *c*) we can use a similar procedure, expanding the heat flux as a double Fourier series. For the strip of Fig. 1(*b*), if there are M nodes along the length and N through the width w, we write

$$q(x, y) = \sum_{i=1}^{M}\sum_{j=1}^{N} a_{ij}\cos\left(\frac{\pi ix}{L}\right)\cos\left(\frac{\pi jy}{w}\right). \tag{17}$$

If the nodes are equally spaced and labelled consecutively along the x axis, reverting to the end $x = 0$ for the next value of y, the coordinates of the kth node are

$$x_k = \frac{L}{M}\bmod(k, M); \quad y_k = \frac{w}{N}\,\text{int}\,(k, M), \tag{18}$$

where int (k, M), mod (k, M) denote the integer quotient and the residual respectively of the ratio k/M.

As in the two-dimensional case, we can then write

$$q_i = \int_0^L\int_0^w q(x, y)W_i(x, y)dydx = B_{ij}\tilde{q}_j, \tag{19}$$

where

$$B_{ij} = \cos\left(\frac{N\pi y_i y_j}{w^2}\right)\cos\left(\frac{M\pi x_i x_j}{L^2}\right). \tag{20}$$

As before, this leads to the eigenvalue equation $\tilde{\mathbf{p}} = fV\tilde{\mathbf{A}}\tilde{\mathbf{p}}$ and we determine the $(NM) \times (NM)$ matrix $\tilde{\mathbf{A}}$ by making (NM) finite element runs for the special heat flux vector $\tilde{q}_j = \delta_{jk}$, $k = 1, (NM)$.

The orthogonality of the Fourier series and the symmetric boundary conditions at $x = 0, L$ ensure that there is no coupling between the various modes in the x-direction, but the traction-free boundary conditions on $y = 0$, w do not lead to a similar decoupling. The matrix $\tilde{\mathbf{A}}$ therefore takes the form

$$\tilde{\mathbf{A}} = \underbrace{\begin{bmatrix} \tilde{\mathbf{A}}^1 & & \\ & \tilde{\mathbf{A}}^2 & \\ & & \ddots \\ & & & \tilde{\mathbf{A}}^M \end{bmatrix}}_{M \times M} \tag{21}$$

where the off-diagonal elements are zero, but each of the $\tilde{\mathbf{A}}^k$ $(k = 1, M)$ is a full $N \times N$ son matrix.

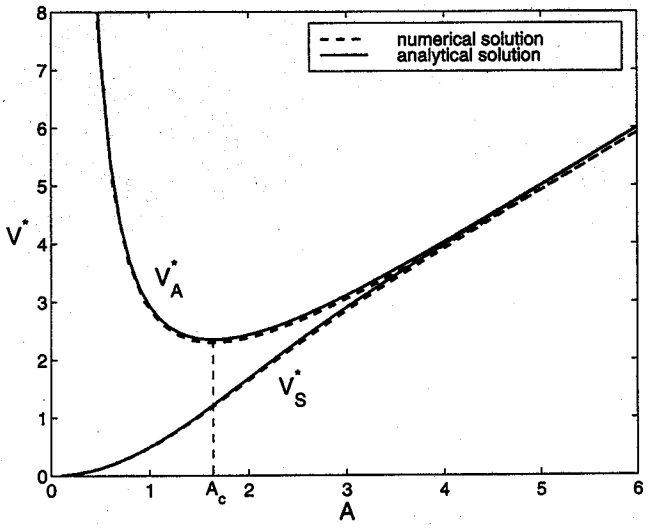

Fig. 2 Comparison of numerical and analytical solutions for the two-dimensional layer model

The eigenvalue problem is therefore partitioned from one of order (NM) to M separate eigenvalues of order N, with a consequent considerable saving of computational effort. More importantly, convergence and conditioning problems associated with the solution of eigenvalue problems for large matrices are avoided, without compromising discretization accuracy.

An essentially similar procedure can be used for the disk geometry of Fig. 1(*c*), with the coordinate θ replacing x/L.

4 Results and Discussion

4.1 The Layer Model. The problem of Fig. 1(*a*) is equivalent to that solved by Lee and Barber (1993) in the limit where the half-planes are rigid nonconductors. This limit can be found analytically by setting $K_1 = 0$, $\alpha_1 = 0$ and $E_1 \to \infty$ in Lee's analysis. After some algebraic manipulations, his equations (68, 69, 76, 77) can then be solved in closed form to yield

$$V_S^* = \frac{fV_S(1 + \nu)\alpha\mu a}{(1 - \nu)K} = \frac{A\sinh(2A)\tanh(A)}{\sinh(2A) + 2A} \tag{22}$$

$$V_A^* = \frac{fV_A(1 + \nu)\alpha\mu a}{(1 - \nu)K} = \frac{A\sinh(2A)\coth(A)}{\sinh(2A) - 2A}, \tag{23}$$

where V_S, V_A are the critical speeds in the symmetric and antisymmetric modes, respectively, $A = ma$ is the dimensionless half-layer thickness, and μ, ν, α, K are the modulus of rigidity, Poisson's ratio, coefficient of thermal expansion, and thermal conductivity respectively for the layer material.

Figure 2 compares the finite element results with Eqs. (22), (23). In the finite element analysis, 4-node linear plane strain elements were used with 20 nodes along the length and 8 through the half-thickness a. Linear elements were used in preference to 8-node quadratic elements to simplify postprocessing, though the latter element type would give better computational accuracy. The finite element results agree very well with the exact solution. Increasing the number of nodes to 50×20 gives curves that are indistinguishable and numerical values within less than 0.2 percent of the analytical values throughout the range.

The antisymmetric curve exhibits a minimum at a critical value $A = A_c$ which can be found by differentiating (23). We obtain

$$\cosh^2(A_c)(\sinh(2A_c) - 2A_c) - 2A_c^2\sinh(2A_c) = 0, \tag{24}$$

with solution $A_c = 1.639$. The corresponding minimum value

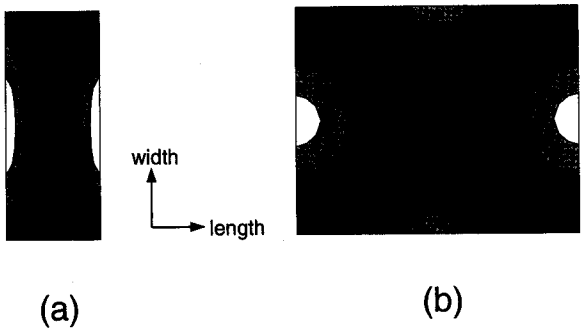

Fig. 3 Dominant modes for the strip model for $w/a = 5$ and (a) $A = 3$, (b) $A = 1$

$V_A^*(A_c) = 2.349$ from Eq. (23). The numerical results of Fig. 2 exhibit a minimum at $A = 1.640$, which again constitutes excellent agreement. This minimum is important in that it will be the first mode to go unstable in situations where only antisymmetric modes can occur. Parametric investigations of Lee's equations have shown that the antisymmetric mode in layer problems is dominant when the elastic modulus of the pad material is low compared with that of the disk (Lam, 1998). For this reason, we concentrate on antisymmetric modes in the following investigation. It should also be noted that the inclusion of realistic pad material properties causes a significant reduction in the value of A_c. For example, Lee and Barber (1993) obtained values of about $A_c = 0.2$ using typical automotive friction material properties.

4.2 The Strip Model. The strip model of Fig. 1(*b*) differs from the layer model in that it supports modes involving variation of contact pressure across the width of the strip and also that the strip has a finite width with traction-free boundary conditions at its edges.

The two-dimensional modes of the layer are modified by the existence of the traction-free boundaries, as shown in Fig. 3(*a*). The temperature and pressure are largely independent of y in the central part of the contact region, leading to an elongated hot spot, but the free edges have the effect of reducing the local variation in pressure, probably due to the lower local stiffness of the structure.

For a given wavenumber A in the x-direction, the critical speed tends to fall with increasing width w. Figure 4 shows the critical speed in the first antisymmetric mode as a function of w for $A = \pi$, normalized with the two-dimensional value V_A of Eq. (23). This wavenumber corresponds to a longitudinal

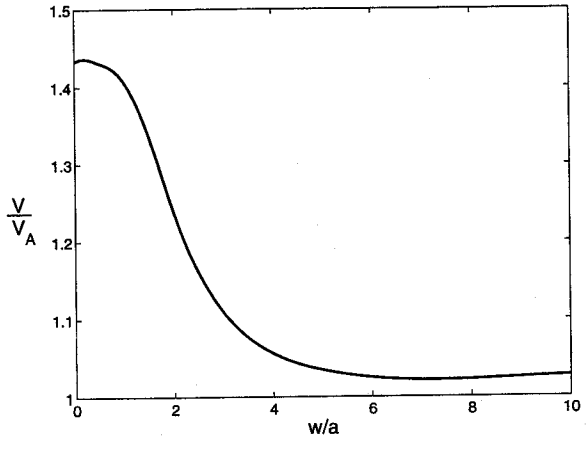

Fig. 4 Effect of width w/a on the critical speed for the first antisymmetric mode of the strip model ($A = \pi$)

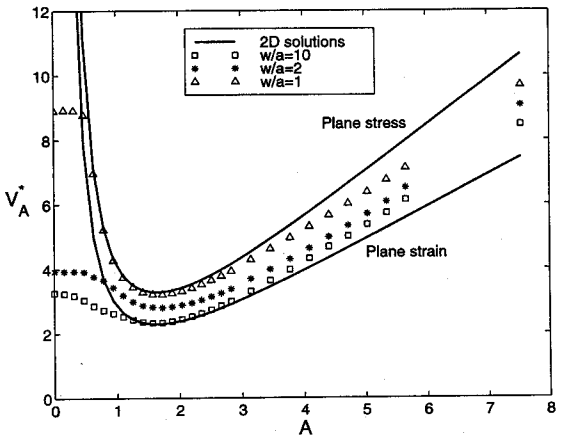

Fig. 5 Critical speed for the first antisymmetric mode of the strip model as a function of wavenumber for various values of the width ratio, w/a

wavelength of $2a$—i.e., the perturbations have a longitudinal wavelength equal to the total strip thickness.

The normalized critical speed approaches unity as w/a increases, as we should expect, since the edge effects in the mode shape of Fig. 3(*a*) then become progressively less important. In practice, it proved difficult to use very large values of w/a in the finite element solution, since it is undesirable to use elements with aspect ratios greater than about 5 and hence large numbers of elements are required. However, the results show convergence to within 3 percent of the plane strain value for $w/a > 6$.

At small values of w/a, the critical speed increases, but there is a limiting value as $w/a \to 0$. In this limit it is natural to make a comparison with the plane stress solution corresponding to Eq. (23). Joachim-Ajao and Barber (1998) have shown that in TEI problems with one body in contact with a rigid plane, the critical speed can be expressed in the dimensionless form

$$\hat{V} = \frac{f V \mu \eta a}{K(\kappa + 1)}, \tag{25}$$

where

$$\kappa = (3 - 4\nu), \quad \eta = \alpha(1 + \nu) \quad \text{for plane strain} \tag{26}$$

and

$$\kappa = \frac{(3 - \nu)}{(1 + \nu)}, \quad \eta = \alpha \quad \text{for plane stress.} \tag{27}$$

We therefore conclude that for all such problems, the ratio

$$\frac{V_{\text{plane stress}}}{V_{\text{plane strain}}} = \left(\frac{(3 - \nu)}{(1 + \nu)} + 1\right)\frac{(1 + \nu)}{(4 - 4\nu)} = \frac{1}{(1 - \nu)}, \tag{28}$$

which for the present case of $\nu = 0.3$ corresponds to a ratio of 1.43. This result agrees very well with the limit of Fig. 4 at small w/a. In fact, for practical purposes, good results are obtained by using the plane stress solution for $w/a \leq 1$, the plain strain solution for $w/a \geq 6$ and a linear interpolation between these values in $1 < w/a < 6$.

Figure 5 shows the antisymmetric critical speed as a function of A for various values of w/a, including the two-dimensional plane strain and plane stress limits from Eqs. (23) and (28). In principle, a single eigenvalue problem for a particular length of strip L yields results for all wavelengths of the form L/k where the wavenumber k is an integer in $(1, M)$. However, the accuracy of the results at higher wavenumber is compromised by the coarse discretization of the associated eigenfunction. The results of Fig. 5 were therefore obtained from a series of runs

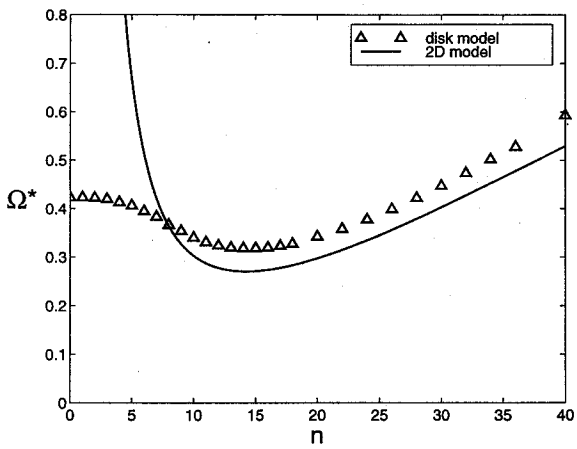

Fig. 6 Critical speed for the first antisymmetric mode of the disk model as a function of wavenumber for $R = 8.7$, $\gamma = 0.354$

in each of which the length L was adjusted to achieve the required wavelength with $k = 1$.

The results show that the strip results monotonically interpolate the plane strain and plane stress results as w/a is increased as long as $A > 1.5$, but at small values of A (large wavelengths) the critical speed is significantly lower than that predicted by the two-dimensional theory. Some insight into this discrepancy is provided by examining the corresponding mode shape. For example, Fig. 3(b) shows the mode shape obtained for a wavelength $L = 2\pi a$, corresponding to $A = 1$ and we notice that there is now a complete wave of pressure variation through the width. Solutions of this kind can persist right down to $A = 0$, which corresponds to modes in which the pressure perturbation is independent of x. In this limit, the modes are analogous to the axisymmetric "banding" modes which are known to occur in disk brakes. By contrast, the mode shape of Fig. 3(a), in which the pressure perturbation has the same sign throughout the width, cannot exist at $A = 0$ because the resulting distribution would violate the requirement that the total perturbation in contact force be zero.

The critical speed in the banding mode ($A = 0$) is generally about 10 percent higher than that corresponding to $A = 2\pi a/w$—i.e., to a Fourier mode in x with wavelength w. This is reasonable, since the pressure variation through the width will be approximately sinusoidal, but the deviations near the edges due to the traction-free boundary condition will cause some increase in critical speed over that associated with a pure sinusoidal mode.

4.3 The Disk Model. We now turn our attention to the disk model of Fig. 1(c), which is the closest approximation to the geometry of actual brakes and clutches here considered. The disk can be characterized by the two dimensionless parameters

$$R = \frac{r_1 + r_2}{2a} = \frac{r_m}{a}; \quad \gamma = \frac{2(r_2 - r_1)}{r_1 + r_2} = \frac{w}{r_m}, \tag{29}$$

where r_m is the mean radius and $w = (r_2 - r_1)$ is the radial width. We also introduce a dimensionless rotational speed

$$\Omega^* = \frac{f(1+\nu)\alpha\mu a^2\Omega}{(1-\nu)K}, \tag{30}$$

where Ω is the rotational speed in radians per second.

The disk is only able to support Fourier modes of the form $\cos(n\theta)$ where n is an integer, so it is natural to present the results in terms of n. Figure 6 shows the antisymmetric critical speed as a function of n for a disk with $R = 8.7$ and $\gamma = 0.354$. Also presented on this figure is the plane strain antisymmetric solution of Eq. (23), based on the velocity and wavenumber at the mean radius, which are related to the disk results by the equations

$$\Omega^* = \frac{V_A^*}{R}; \quad n = RA. \tag{31}$$

As with the strip results of Fig. 5, there is reasonable agreement with the plane strain solution for large wavenumber, but significant deviation below the minimum point, which in the present case occurs at $n \equiv n_c = 14$. The critical speed is a weak function of n near n_c, suggesting that modes in the range $10 < n < 18$ might be excited at the initiation of instability.

A significant difference between the disk and strip models is that in the former case, the sliding speed is a function of radius, being given by $r\Omega$. This affects both the critical speed and the eigenmode, causing the hot spots to migrate towards the outer radius. As we might expect, this effect is more pronounced when γ is large, corresponding to a larger ratio r_2/r_1. Figure 7 shows the effect of γ on the mode shape for $n = 14$ and $R = 8.7$. When γ is small and n is large, sectors of the disk act essentially like sections of the strip and the modes are similar to those shown in Fig. 4.

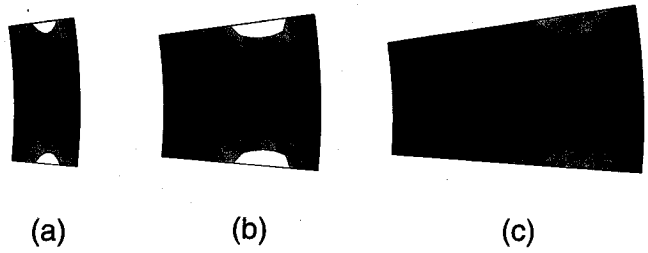

Fig. 7 Effect of the radial width ratio $\gamma = w/r_m$ on mode shape for $n = 14$ and $R = 8.7$. (a) $\gamma = 0.10$, (b) $\gamma = 0.25$, (c) $\gamma = 0.40$

Figure 8 shows the critical rotational speed in the first antisymmetric mode as a function of γ for $n = 14$ and $R = 8.7$. These results are normalized by the corresponding plane strain results, defined by Eqs. (31). The critical speed decreases with increasing γ as we might expect by comparison with the strip results of Fig. 5. However, the critical speeds obtained are always somewhat lower than those obtained for the strip and therefore fall below the plane strain value at large γ. This is probably attributable to the fact that stability is then governed by a hot spot displaced toward the outer radius at which the linear sliding speed is increased.

For a given value of γ, the parameter R is an inverse measure of the disk thickness. Generally, the dominant wavelength is

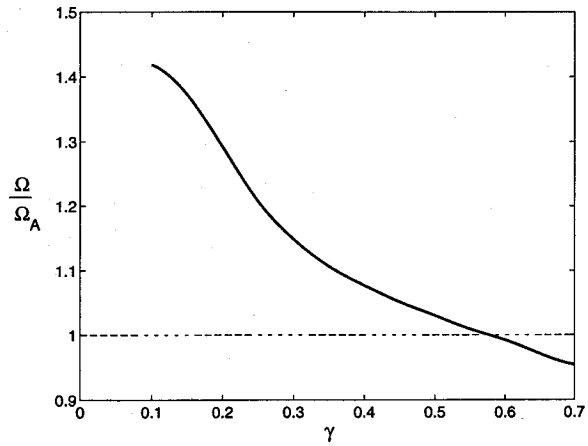

Fig. 8 Effect of γ on the critical speed for the first antisymmetric mode of the disk model ($n = 14$, $R = 8.7$)

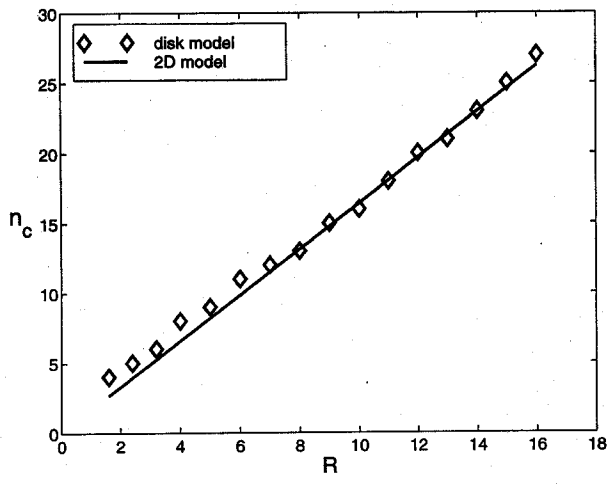

Fig. 9(*a*)

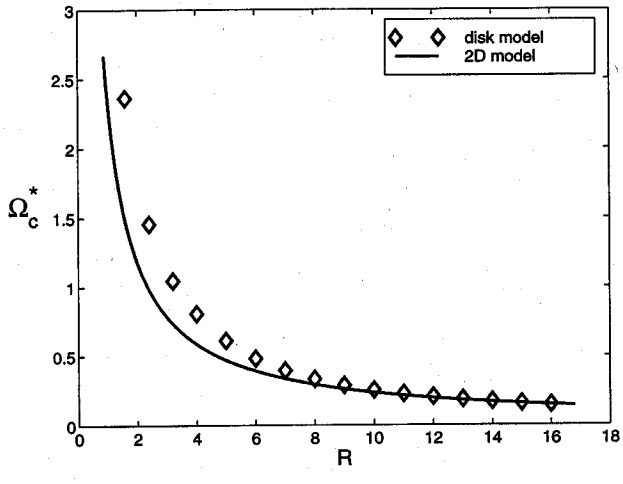

Fig. 9(*b*)

Fig. 9 (*a*) Critical wavenumber, n_c, and (*b*) the corresponding critical speed Ω_c^* as functions of R, for $\gamma = 0.345$. The solid lines represent predictions based on the two-dimensional plane strain solution.

proportional to the disk thickness and hence the number of hot spots predicted around the circumference, n_c, is proportional to R. We anticipate the greatest deviation from the two-dimensional and strip results when n_c is small and hence when the angle subtended between adjacent hot spots is relatively large. Figure 9 presents (a) n_c and (b) the corresponding critical speed Ω_c^* as functions of R, for $\gamma = 0.345$. The solid lines in these figures represent predictions based on the two-dimensional plane strain solution, which take the form

$$n_c = 1.639R; \quad \Omega_c^* = \frac{2.349}{R} \tag{32}$$

In Fig. 9(*a*), we note that the disk results are necessarily discontinuous, because n_c is restricted to integer values, whereas the corresponding two-dimensional curve is continuous. However, with this caveat, Eq. (32) gives an extremely good approximation to the three-dimensional disk results even for quite small values of R.

Figure 9(*b*) shows that Eq. (32) underestimates Ω_c^* for the disk at small R, but the error is still relatively modest. For example, at $R = 2.4$, where $n_c = 4$, Ω_c^* is underestimated by 32.7 percent. At large values of R, Eq. (32) gives a very good approximation to disk results.

5 Conclusions

The results of this analysis show that some interesting new effects appear as the correct three-dimensional geometry of the brake disk is taken into account. The hot spots generally become focal in shape and modes with several reversals through the width start to become dominant at small axial wavenumbers, including a 'thermal banding' mode corresponding to $n = 0$. Also, the dependence of sliding speed on radius causes focal hot spots to migrate towards the outer radius for disks with significant radial width.

However, the most striking conclusion is that, excluding banding modes, the dominant wavelength (hot spot spacing) and critical speed remain quite well predicted by the two-dimensional analysis of Eqs. (22)–(24), even when the number of hot spots is relatively small. Furthermore, the most significant deviation from the two-dimensional analysis can be described as a monotonic interpolation between the two-dimensional critical speeds for plane stress and plane strain as the width w of the sliding surface is increased. Most practical brake and clutch disks have widths in the range $w/a > 6$, for which the plane strain solution is a good approximation.

This conclusion promises well for the development of algorithms for design against TEI, since the two-dimensional problem can in many cases be treated analytically (Lee and Barber, 1993), permitting extensive parametric investigation and optimization without incurring excessive computational costs.

Acknowledgments

The authors are pleased to acknowledge support from the Ford Motor Company and from the National Science Foundation under contract number CMS-9619527.

References

Anderson, A. E., and Knapp, R. A., 1990, "Hot Spotting in Automotive Friction Systems," *Wear,* Vol. 135, pp. 319–337.

Barber, J. R., 1967, "The Influence of Thermal Expansion on the Friction and Wear Process," *Wear,* Vol. 10, pp. 155–159.

Barber, J. R., 1969, "Thermoelastic Instabilities in the Sliding of Conforming Solids," *Proc. Roy. Soc.,* Vol. A312, pp. 381–394.

Burton, R. A., Nerlikar, V., and Kilaparti, S. R., 1973, "Thermoelastic Instability in a Seal-Like Configuration," *Wear,* Vol. 24, pp. 177–188.

Dow, T. A., and Burton, R. A., 1972, "Thermoelastic Instability of Sliding Contact in the Absence of Wear," *Wear,* Vol. 19, pp. 315–328.

Du, Shuqin, Zagrodzki, P., Barber, J. R., and Hulbert, G. M., 1997, "Finite Element Analysis of Frictionally-Excited Thermoelastic Instability," *J. Thermal Stresses,* Vol. 20, pp. 185–201.

Hartsock, D. L., Hecht, R., and Fash, J. W., 1997, "Parametric Analyses of Thermal Elastic Instability in Disc Brakes," Ford Motor Company, Technical Report SR-97-159.

Inoue, H., 1986, "Analysis of Brake Judder Caused by Thermal Deformation of Brake Disk Rotors," SAE 865131.

Joachim-Ajao, D., and Barber, J. R., 1998, "Effect of Material Properties in Certain Thermoelastic Contact Problems," ASME *Journal of Applied Mechanics,* Vol. 65, pp. 889–893.

Johnson, K. L., 1985, *Contact Mechanics,* Cambridge University Press, Cambridge, pp. 123–124.

Kreitlow, W., Schrödter, F., and Matthäi, H., 1985, "Vibration and Hum of Disc Brakes Under Load," SAE 850079.

Lam, K. B., Private communication.

Lee, Kwangjin, and Barber, J. R., 1993, "Frictionally-Excited Thermoelastic Instability in Automotive Disk Brakes," ASME JOURNAL OF TRIBOLOGY, Vol. 115, pp. 607–614.

Lee, Kwangjin, and Dinwiddie, Ralph B., 1998, "Conditions of Frictional Contact in Disk Brakes and Their Effects on Brake Judder," SAE 980598.

Zagrodzki, P., 1990, "Analysis of Thermomechanical Phenomena in Multidisc Clutches and Brakes," *Wear,* Vol. 140, pp. 291–308.